Published in final edited form as:
Curr Biol. 2010 November 23; 20(22): 2052–2057. doi:10.1016/j.cub.2010.10.025.

Synchronized neural input shapes stimulus selectivity in a collision-detecting neuron

Peter W. Jones[1] and **Fabrizio Gabbiani**[1,2,*]

[1] Department of Neuroscience, Baylor College of Medicine, One Baylor Plaza, Houston, TX 77030, USA

[2] Department of Computational and Applied Mathematics, Rice University, 6100 Main, Houston, TX 77005, USA

Summary

How higher-order sensory neurons generate complex selectivity from their simpler inputs is a fundamental question in neuroscience. The lobula giant movement detector, LGMD, is an identified, higher-order visual neuron in the locust, *Schistocerca americana*, that responds selectively to objects approaching on a collision course or their two-dimensional projections, referred to as looming stimuli [1,2,3,4]. To study how this selectivity arises, we designed an apparatus allowing us to stimulate, individually and independently, a sizable fraction of the ~15,000 elementary visual inputs impinging retinotopically onto the LGMD's large dendritic fan [5,6,7] (Figure 1A*i*). We then recorded intracellular signals *in vivo* throughout the visual pathway, assessing the LGMD's activity and that of all three successive pre-synaptic stages conveying local excitatory inputs. Our results suggest that as collision becomes increasingly imminent, the strength of individual excitatory LGMD inputs increases, while their latency decreases. This latency decrease favors summation of inputs activated sequentially throughout the object approach, making the neuron maximally sensitive to collision-bound trajectories. Thus, the LGMD's selectivity arises – at least in part – from presynaptic mechanisms that synchronize a large population of inputs during the approach of an object on a collision course and subsequent detection by postsynaptic mechanisms within the neuron itself. Analogous mechanisms are likely to underlie the tuning properties of visual neurons in other species as well.

Results

We took advantage of the fact that locusts possess apposition compound eyes, and thus the photoreceptors within each ommatidium (facet) comprise a single functional unit [8]. We designed a custom microscope to deliver independent focal stimulation to ~300 facets on the eye (Figure S1). This allowed us to control ~5% of the excitatory synaptic inputs to the LGMD, while maintaining the ability to record intracellularly from neurons of the excitatory pathway *in vivo*. Additionally, this apparatus also allowed us to decompose looming stimuli into their elementary visual components, due to the discrete sampling inherent to the ommatidial eye lattice. We verified individual facet stimulation on the eye by mapping the receptive fields of single photoreceptors. A representative receptive field is shown overlaid

*Corresponding author: gabbiani@bcm.edu, 1-713-798-1849.

on an image of the eye in Figure 1B*iii*, along with membrane potential traces from which it was generated (Figure 1B*i*-*ii*).

The logarithmic speed-dependence of LGMD's excitation [9] suggests correlation-type interactions between retinotopic inputs having adjacent receptive fields (Figure 1A*ii*). In fact, a model of the LGMD endowed with such interactions reproduces several of its response characteristics [10]. Such mirror symmetric correlation detectors comprise the Reichardt model of motion detection in insects [11,12], which is closely related to motion detection algorithms postulated in higher vertebrates [13]. Alternatively, the presynaptic inputs to the LGMD may act largely independently of each other (Figure 1A*iii*) [14,4]. Testing these hypotheses requires precise control over individual retinotopic inputs [11,12], as achieved by our microscope.

LGMD responses to stimulation of individual facets showed a transient depolarization to brightness changes, with slightly stronger OFF than ON responses (mean: 8.4, 7.4 mV; SE: 0.91, 0.81 mV; n = 22, 12 facets in 6 animals, respectively) [6]. Although this difference was not statistically significant ($p = 0.45$, t-test), it may be amplified during the presentation of looming stimuli, when several thousand facets are activated. This may contribute to the stronger LGMD responses elicited by dark rather than bright looming stimuli [4]. To probe for the presence of correlation type input to the LGMD, we delivered apparent motion stimuli consisting of ON or OFF light pulses with variable delays to two adjacent facets on the eye (Figure 1C*i*-*iv*). The presence of correlator-type circuitry predicts a non-linear response peak at an inter-stimulus interval matching the correlation detector's effective neural delay. We thus computed a summation index (SI, see Methods) to identify responses higher than those expected from the sum of the two inputs delivered in isolation. No such non-linear response increases could be found (Figure 1D), suggesting that no correlation mechanism exists within the LGMD's excitatory input. We also tested the directionality of apparent motion responses (Figure S1), since single correlation detectors are inherently directionally selective, and cells receiving correlation detector input often are as well [15,12]. We found no evidence for direction selectivity, consistent with a lack of correlation detector input to the LGMD.

An alternative mechanism that could result in speed sensitivity of the LGMD's excitatory input is illustrated in Figure 2A. The faster the movement of a dark edge across a photoreceptor's receptive field (Figure 2A*i*), the more rapidly the luminance encountered by the receptor will decrease (Figure 2A*ii*). If such luminance changes were faithfully transduced and the resulting response slopes extracted, it would yield a local signature of stimulus speed. To test this hypothesis, we presented edges drifting at speeds covering the dynamic range sensed by the LGMD neuron [9] and recorded single photoreceptor responses. We found that the response slopes indeed correlated with edge speed (Figure 2B; $\rho = -0.86$, $p = 8.6 \times 10^{-22}$). Next, we designed single facet stimuli consisting of luminance decreases (Figure 2C) and adjusted their duration to cover the range of photoreceptor response slopes elicited by moving edges. The slopes could be closely matched (Figure 2D), although the response transients were not exactly identical due to minor stimulus brightness and stimulation protocol differences (Figure S2). Recordings from large monopolar cells (LMCs) in the lamina, which are most likely the next stage of the visual pathway [16], revealed that these neurons responded with increasing depolarization as the slope of the photoreceptor response became more negative (Figure 2E). Thus, our results establish that in the locust these neurons effectively extract the slope of the photoreceptor response, consistent with the high-pass filtering properties reported in other insect species [17,18]. Importantly, we also found that the delay of the peak response decreased as the stimulus duration became shorter. Since recording from the transmedullary neurons that synapse onto the LGMD is not yet technically feasible, we probed that stage of the excitatory pathway by

voltage-clamping the LGMD. We could successfully resolve excitatory postsynaptic currents elicited by single facet stimulation and found that their strength and latency also depended on the time course of the associated luminance change (Figure 2F). In current clamp, the LGMD's membrane potential depolarizations elicited by single facet stimulation had similar properties, except for a broadening, presumably caused by the filtering associated with the neuron's membrane time constant (Figure 2G). Thus the decrease in response latency was consistently maintained from the sensory periphery to the LGMD (Figure 2H). Remarkably, the strongest single facet stimuli could reliably elicit a few spikes in the LGMD, which occurred with precise timing (Figure 2G). The mean difference in first spike latency for all stimulus-induced spikes was 4.6 ms (SD = 3.5 ms, n = 50 trials).

These results suggest a mechanism that could tune the LGMD neuron to looming stimuli. As illustrated in Figure 3A, if an object approaches on a collision course at constant velocity, v, the angular speed, θ', of its expanding edges increases non-linearly with time, because the subtended half-angle, θ, is given by $\tan\theta = l/vt$, where t is time to collision and l is the object's half size [19]. This in turn will cause increasingly rapid luminance changes as facets are stimulated in quick succession (Figure 3A*i*-*iii*), and will tend to synchronize the resulting excitatory input impinging onto the LGMD (Figure 3A*iv*). We tested this hypothesis by disrupting the orderly sequence of luminance changes over single facets, either by randomly shuffling their order of appearance or by keeping the duration of each luminance change constant (Figure 3A*v*-*vi*). First, we tested the effect of shuffling the sequence on a local scale by selecting an array of 3×15 facets and stimulating them sequentially with increasingly fast luminance changes, mimicking a looming stimulus edge during expansion at fast, medium or slow speeds. We recorded LGMD responses to these "pseudo-looming" stimuli and compared them to responses to corresponding shuffled stimuli. Since these stimulus differences might also modulate feedforward inhibition [20], we performed these experiments after local application of the selective $GABA_A$ antagonist picrotoxin to isolate the excitatory input to the LGMD. As illustrated in Figure 3C, we observed that the peak firing rates elicited in response to pseudo-looming stimuli were larger than in the corresponding shuffled conditions. In a subset of neurons, we also obtained intracellular recordings, which showed a similar attenuation of the peak membrane potential.

To further test this synchronization hypothesis on a larger and behaviorally relevant spatial scale [21,22], we used a monitor for visual stimulation at the expense of the ability for precise, single facet stimulation. We designed a "coarse" looming stimulus by discretizing visual space within 3º×3º regions, approximately of the same size as single photoreceptors' receptive fields [23]. During a coarse loom, the time course of the luminance change in each of these "pixels" matched that elicited by a looming stimulus, integrated over the pixel's area. As expected from the fact that this discretization matched the spatial resolution of the locust compound eye, responses to coarse looming stimuli were similar to those elicited by conventional looming stimuli (Figure S3). To disrupt the synchronization of individual inputs impinging onto the LGMD, we adopted the strategy illustrated in Figure 3A*vi*. Namely, we fixed the luminance change time course of all individual pixels to the average of the coarse stimulus and adjusted their onset times so as to closely reproduce the whole screen luminance time course of the looming stimulus (Figure S4). We denote these stimuli by "constant rate" looming stimuli, since the rate of luminance transition is fixed over time. In Figure 4, we compare the LGMD responses to the coarse looming stimuli with those elicited by constant rate looming stimuli, for three values of the stimulus size to speed ratio, $l/|v|$, characterizing the time course of the approach angle. As can be seen from both the single neuron spike trains (Figure 4A) and the population averages, constant rate looming stimuli evoked much attenuated responses compared to coarse looming, when measured either by the peak firing rate or the spike count (Figure 4B, C). Additionally, the timing of the response peak, which signals an angular threshold size that is behaviorally relevant for

collision avoidance behaviors [24,25], was disrupted for the constant rate looms. Specifically, response peaks occurred earlier relative to collision time for constant rate stimuli (Figure 4D), causing angular threshold sizes [19] to change from 21.2° for coarse looming to 9.8° for constant rate.

Discussion

These results suggest that synchronization of the excitatory synaptic inputs impinging onto the LGMD's fan-shaped dendrite indeed plays an important role in tuning the neuron to looming stimuli. In this pathway, synchronization arises through a decrease in the latency of excitatory inputs as the instantaneous angular speed of the edges sweeping across individual photoreceptor receptive fields increases. Edge acceleration is in turn a defining feature of looming stimuli, entailing specificity to this mechanism. While edge acceleration had previously been recognized as important for sustained LGMD responses [4,26] and several mechanisms capable of reducing responses to its non-preferred stimuli had been identified [20,26,27,28], no mechanism specifically facilitating responses to accelerating or looming stimuli was known.

The synchronization mechanism unveiled by our experiments appears to rely chiefly on the temporal coherence of signals across individual facets. Indeed, we found no evidence for correlation-type motion detection circuitry that would enhance responses to the spatio-temporal coherence of a stimulus on a fine scale, across adjacent facets. Our results do not rule out, however, that the spatial coherence of looming stimuli may also contribute to the looming sensitivity of the LGMD. For example, excitatory or inhibitory input strength could be modulated by spatio-temporal coherence at larger scales than that detected by correlation of signals across adjacent facets.

Both experimental and theoretical arguments have implicated synchronization of synaptic input in the tuning of mammalian visual neurons [29,30,31], suggesting that analogous mechanisms may be at work. The postsynaptic detection of such neural synchrony could be based on the spatial specificity of synaptic inputs [32] in the locust visual system [6] and in other species [33, but see 34]. Our results show that the systematic mapping of individual presynaptic neural components within well-defined neural circuits is a powerful tool to explain how the complex tuning properties of higher order neurons arise *in vivo*.

Experimental Procedures

Animal dissection and electrophysiology

Locusts were mounted in a plastic holder and dissected as previously described [35]. Sharp microelectrodes were used for intracellular recordings from photoreceptors, LMCs (80–240 MΩ, 2M KAc/0.5M KCl), and the LGMD (8–30 MΩ, 2M KAc/0.5M KCl or 3M KCl for voltage clamp). Intracellular signals were low-pass filtered (V_m: 10 kHz, I_m: 5 kHz) and digitized (20 kHz). Photoreceptor and LGMD recordings used borosilicate electrodes (1.2/0.8 mm and 1.2/0.5 OD/ID, respectively; WPI) while LMC recordings used aluminosilicate (1.0 OD; Harvard Apparatus). An Ag/AgCl wire was used as reference. Current clamp recordings were made in discontinuous current clamp (DCC, ~25 kHz switching frequency) or bridge mode. Voltage-clamp recordings from the LGMD used discontinuous single-electrode voltage clamp (dSEVC, ~25 kHz switching amplifier, NPI). All dSEVC electrodes had <20 MΩ resistances, and electrode resistance (bridge) or capacitance (DCC/dSEVC) were fully compensated in the bath, immediately prior to tissue penetration. Intracellular recordings were obtained from the lobula and lamina through the desheathed optic lobe and from the retina through a small (~50μm × 50μm) hole just below the dorsal rim of the eye. Photoreceptor recordings were identified by their resting potential

(~ −50mV) and depolarizing responses to luminance increases. The extracellular potential of the lamina modulates in phase with a flashing light stimulus allowing identification of LMCs by a slight resting hyperpolarization and transient, anti-phase responses to light flashes. LGMD recordings were identified by the cell's 1:1 spike correspondence with the simultaneously recorded DCMD [36]. The cell was penetrated in the proximal region of the excitatory dendritic field, with spike heights varying between 20–50 mV. Stable LGMD recordings could be maintained for typically >60 minutes. Extracellular signals were acquired as previously described. DCMD spikes were detected by thresholding and instantaneous firing rates were calculated by convolving individual spike trains with a Gaussian window (σ=20 ms).

Injection of PCTX in the lobula

Prior to pseudo-looming experiments, small volumes of picrotoxin (PCTX, 10 mM) in aqueous solution were injected into the lobula to block feedforward inhibition onto the LGMD [21]. Fast green (0.5%) was used for injection visualization. The injection pipettes had tip diameters of ~2μm, and were visually positioned against the posterior dorsal aspect of the lobula using a micromanipulator, close enough so that the injections penetrated the tissue. PCTX acted quickly (< 1 min), with LGMD responses to visual stimuli increasing markedly. Only the lobula was stained by the injection, making it unlikely that the medulla or lamina neuropils (located several 100 μm away) were affected. Additionally, the pipettes were placed into the bath only immediately before injection, were removed immediately after, and the saline was exchanged to prevent diffusion through the bath to other brain areas.

Visual stimulation

Visual stimuli were generated using custom software on a PC running a real-time operating system (QNX 4). Wide-field dark (2 cd/m^2) and bright (90 cd/m^2) stimuli were presented on a CRT monitor (200 Hz). Single ommatidium resolution stimulation was achieved by projecting an image generated using a DLP projector (NEC LT140) through a custom-built microscope mounted horizontally on a vibration isolated optical table (illuminance range: 4–2530 lux). Both displays were calibrated to ensure linear, 6-bit resolution control over light levels. Single facet and pseudo-looming experiments used a 20x/0.5 NA and a 10x/0.3 NA water immersion objective, respectively. A watertight plastic cup was placed around the objective, sealed to the animal holder with silicone grease, and the animal's right eye was submerged in water (to neutralize the optical power of the facet lens) for imaging and stimulation. The focal plane was set behind the cornea.

Single facet and apparent motion stimuli

Each stimulus spot was 2×2 pixels (5 μm × 5 μm) in size, positioned in the center of each ommatidium. Each stimulus was a 1500 ms light pulse from baseline (4 lux) to a variable maximum (≤2530 lux). Luminance changes had the time course of a cumulative Gaussian, with their mean and two standard deviations equal to half the transition duration. Multiple facets/adjacent facet pairs were stimulated when recording from the LGMD (4 maximum, with at least 2 intermediate facets). Each facet was stimulated less than once per minute to avoid local habituation. Stimuli were presented every 5 seconds for LMC and photoreceptor experiments. Trial types within all experiments were pseudo-randomly interleaved.

Pseudo-looming stimuli

The stimuli spanned three facet rows, each 15 facet long, with each stimulus point positioned over a single facet. The stimulus points along each row were illuminated in sequence, with the onsets of luminance changes one frame (1/60 s) apart, over a period of

233 ms (Figure S4). The duration of luminance changes for single facets were chosen to span the range to which the LGMD is sensitive, and progress through that range at different rates. The progression of luminance changes was chosen to mimic the acceleration caused by a looming edge, while the constant interval between stimulus point onsets allowed for a dissociation of stimulus progression across the retina (number of facets stimulated over a period of time) and luminance change at single points, which is not possible using an actual moving edge. The shuffled condition pseudo-randomly reassigned the time course of luminance changes across stimulus points, with the constraint that for each frame, the mean duration of luminance changes for the three stimulated facets lie within 20–80% of the range of luminance change durations. This condition prevented the fastest luminance changes from occurring simultaneously, as in the pseudo-looming stimuli. In every experiment, each facet was stimulated individually to confirm that there was no positional bias in response strength that could cause a difference between pseudo-looming and shuffled conditions. Stimuli were presented every 40 seconds.

Constant rate looming

To construct the "constant rate" looming stimuli, we first created a looming stimulus with a spatial resolution matching that of the locust eye (3º×3º pixels; 729 pixels total, covering 85°×85°). In this stimulus (coarse looming), each pixel's luminance follows the same time course as the luminance of the simulated approaching object integrated over its area. To create the constant rate loom, we constrained the luminance change of each pixel to have a duration equal to the mean across pixels during the coarse loom. We then adjusted each pixel's luminance change onset time to match the temporal profile of the whole screen luminance during the normal looming stimulus. Stimuli were presented once per minute.

Data analysis and statistics

Data analysis was carried out using custom MATLAB programs (MathWorks). The nonparametric Wilcoxon rank-sum test (denoted p_{RS}) was employed for comparisons of two independent data sets for the pseudo-looming experiments, while a Kruskal-Wallis test (p_{KW}) followed by Tukey's honestly significant difference test (p_{HSD}) was used for looming experiments where 3 conditions were compared. LGMD current clamp recordings were median- ltered (8 ms window) for spike removal. Summation indices were calculated as $SI=R_{both}/(R_{facet1} + R_{facet2})$ with R being the peak of the median-filtered V_m traces.

Supplementary Material

Refer to Web version on PubMed Central for supplementary material.

Acknowledgments

We would like to thank Drs. H. Krapp, J. Maunsell, H. Ogmen, P. Saggau, and S. Peron for comments. This work was supported by grants from the National Science Foundation and the National Institute of Mental Health.

References

1. Schlotterer GR. Response of the locust descending movement detector neuron to rapidly approaching and withdrawing visual stimuli. Can J Zool. 1977; 55:1372–1376.
2. Rind FC, Simmons PJ. Orthopteran DCMD neuron: a reevaluation of responses to moving objects. I. Selective responses to approaching objects. J Neurophysiol. 1992; 68:1654–1666. [PubMed: 1479436]
3. Hatsopoulos N, Gabbiani F, Laurent G. Elementary computation of object approach by a wide-field visual neuron. Science. 1995; 270:1000–1003. [PubMed: 15290817]

4. Simmons PJ, Rind FC. Orthopteran DCMD neuron: a reevaluation of responses to moving objects. II. Critical cues for detecting approaching objects. J Neurophysiol. 1992; 68:1667–1682. [PubMed: 1479437]
5. Strausfeld, NJ.; Nässel, DR. Neuroarchitectures serving compound eyes of crustacea and insects. In: Autrum, H., editor. Comparative physiology and evolution of vision of invertebrates, B: Invertebrate visual centers and behavior I, Handbook of sensory physiology. Vol. 7. Berlin: Springer Verlag; 1981. p. 1-132.
6. Peron SP, Jones PW, Gabbiani F. Precise subcellular input retinotopy and its computational consequences in an identified visual interneuron. Neuron. 2009; 63:830–842. [PubMed: 19778511]
7. Rind FC, Simmons PJ. Local circuit for the computation of object approach by an identified visual neuron in the locust. J Comp Neurol. 1998; 395:405–415. [PubMed: 9596531]
8. Shaw SR. Organization of the locust retina. Symp Zool Soc Lond. 1968; 23:135–163.
9. Krapp HG, Gabbiani F. Spatial distribution of inputs and local receptive field properties of a wide-field, looming sensitive neuron. J Neurophysiol. 2005; 93:2240–2253. [PubMed: 15548622]
10. Harrison RR. A biologically inspired analog IC for visual collision detection. IEEE Trans Circuits and Systems. 2005; 52:2308–2318.
11. Reichardt W. Evaluation of optical motion information by movement detectors. J Comp Physiol A. 1987; 161:533–547. [PubMed: 3681769]
12. Single S, Haag J, Borst A. Dendritic computation of direction selectivity and gain control in visual interneurons. J Neurosci. 1997; 17:6023–6030. [PubMed: 9236213]
13. Bradley DC, Goyal MS. Velocity computation in the primate visual system. Nat Rev Neurosci. 2008; 9:686–695. [PubMed: 19143050]
14. Rowell CH, O'Shea M. The neuronal basis of a sensory analyser, the acridid movement detector system. I. Effects of simple incremental and decremental stimuli in light and dark adapted animals. J Exp Biol. 1976; 65:273–288. [PubMed: 1003082]
15. Haag J, Borst A. Neural mechanism underlying complex receptive field properties of motion-sensitive interneurons. Nat Neurosci. 2004; 7:628–634. [PubMed: 15133514]
16. James AC, Osorio D. Characterisation of columnar neurons and visual signal processing in the medulla of the locust optic lobe by system identification techniques. J Comp Physiol A. 1996; 178:83–99.
17. Laughlin SB, Hardie RC. Common strategies for light adaptation in the peripheral visual systems of fly and dragonfly. J Comp Physiol A. 1978; 128:319–340.
18. Juusola M, Uusitalo RO, Weckström M. Transfer of graded potential at the photoreceptor-interneuron synapse. J Gen Physiol. 1995; 105:117–148. [PubMed: 7537323]
19. Gabbiani F, Krapp HG, Laurent G. Computation of object approach by a wide-field, motion-sensitive neuron. J Neurosci. 1999; 19:1122–1141. [PubMed: 9920674]
20. Gabbiani F, Cohen I, Laurent G. Time-dependent activation of feed-forward inhibition in a looming-sensitive neuron. J Neurophysiol. 2005; 94:2150–2161. [PubMed: 15928055]
21. Gabbiani F, Krapp HG, Koch C, Laurent G. Multiplicative computation in a visual neuron sensitive to looming. Nature. 2002; 420:320–324. [PubMed: 12447440]
22. Fotowat H, Gabbiani F. Relationship between the phases of sensory and motor activity during a looming-evoked multistage escape behavior. J Neurosci. 2007; 27:10047–10059. [PubMed: 17855619]
23. Wilson M. Angular sensitivity of light and dark adapted locust retinula cells. J Comp Physiol. 1975; 97:323–328.
24. Santer R, Rind FC, Stafford R, Simmons P. Role of an identified looming-sensitive neuron in triggering a flying locust's escape. J Neurophysiol. 2006; 95:3391–3400. [PubMed: 16452263]
25. Fotowat, H.; Harrison, RR.; Gabbiani, F. Mechanisms of sensorimotor integration underlying visually guided escape behaviors. 2010. Submitted
26. Peron SP, Gabbiani F. Spike frequency adaptation mediates looming stimulus selectivity in a collision-detecting neuron. Nat Neurosci. 2009; 12:318–326. [PubMed: 19198607]
27. O'Shea M, Rowell CH. Protection from habituation by lateral inhibition. Nature. 1975; 254:53–55. [PubMed: 1113876]

28. Zaretsky M. Quantitative measurements of centrally and retinally generated saccadic suppression in a locust movement detector neurone. J Physiol. 1982; 328:521–533. [PubMed: 7131324]

29. Monier C, Chavane F, Baudot P, Graham LJ, Frégnac Y. Orientation and direction selectivity of synaptic inputs in visual cortical neurons: a diversity of combinations produces spike tuning. Neuron. 2003; 37:663–680. [PubMed: 12597863]

30. Priebe NJ, Ferster D. Direction selectivity of excitation and inhibition in simple cells of the cat primary visual cortex. Neuron. 2005; 45:133–145. [PubMed: 15629708]

31. Wang HS, Spencer D, Fellous JM, Sejnowski TJ. Synchrony of thalamocortical inputs maximizes cortical reliability. Science. 2010; 328:106–109. [PubMed: 20360111]

32. Polsky A, Mel BW, Schiller J. Computational subunits in thin dendrites of pyramidal cells. Nat Neurosci. 2004; 7:621–627. [PubMed: 15156147]

33. Bollmann JH, Engert F. Subcellular topography of visually driven dendritic activity in the vertebrate visual system. Neuron. 2009; 61:895–905. [PubMed: 19323998]

34. Jia H, Rochefort NL, Chen X, Konnerth A. Dendritic organization of sensory input to cortical neurons in vivo. Nature. 2010; 464:1307–1312. [PubMed: 20428163]

35. Peron SP, Krapp HG, Gabbiani F. Influence of electrotonic structure and synaptic mapping on the receptive field properties of a collision-detecting neuron. J Neurophysiol. 2007; 97:159–177. [PubMed: 17021031]

36. O'Shea M, Rowell CH. The neuronal basis of a sensory analyser, the acridid movement detector system II: response decrement, convergence, and the nature of the excitatory afferents to the fan-like dendrites of the LGMD. J Exp Biol. 1976; 65:289–308. [PubMed: 187712]

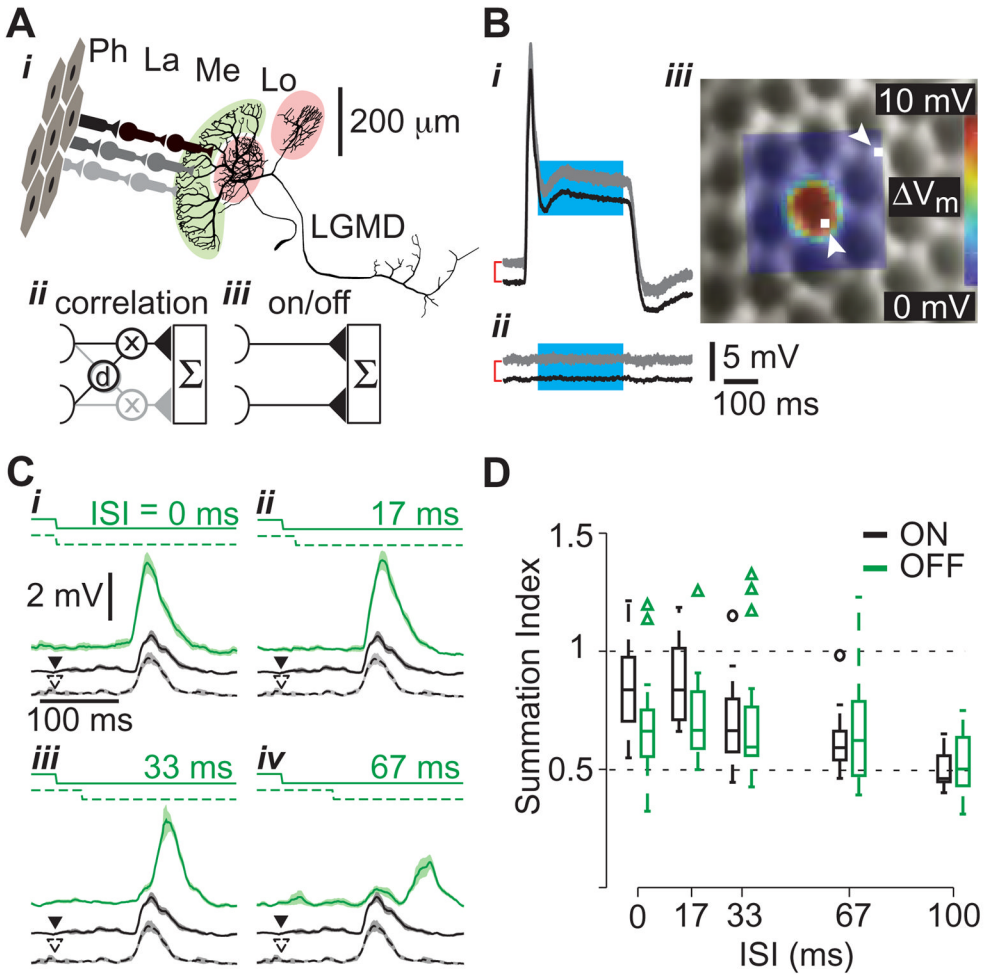

Figure 1. Probing motion detection mechanisms using visual stimuli with single facet resolution

A *i* Excitatory neural circuitry presynaptic to the LGMD. Photoreceptors (Ph), located within ommatidia (facets), synapse on cells in the lamina (La), which in turn contact medullary neurons (Me) that synapse onto the LGMD in the lobula (Lo). These inputs impinge on LGMD's large dendritic fan (highlighted in light green) while two separate dendritic fields receive inhibitory inputs (light red; scale bar applies to LGMD only). The correlation diagram (***ii***) illustrates hypothetical delay (d) and multiply (x) interactions between adjacent LGMD inputs (one input in black, the other gray), in contrast to independent input channels (***iii***). Both models include summation (Σ) in the LGMD. **B** Single photoreceptor responses (gray, n=3 trials) and mean (black) to a 5×5 μm stimulus positioned on a visually identified ommatidium (***i***) and beside one (***ii***). For clarity, the mean responses have been shifted vertically (red brackets, subsequent offsets left unmarked). ***iii*** Receptive field (RF) of a photoreceptor, mapped using a 20×20 location grid, superimposed on the simultaneously acquired microscopic image of the eye lattice. White squares, indicated by arrowheads, show the stimulation locations corresponding to the traces in *i* and *ii*. The RF was constructed by averaging over the cyan section of the traces in *i* and *ii*. The diameter of an ommatidium is ~25 μm. **C** LGMD responses to apparent motion stimuli. Two adjacent facets were stimulated by a luminance step decrease with varying inter-stimulus intervals (ISIs; top solid and dashed lines in ***i-iv***). The LGMD response is illustrated below the stimulus in green (median filtered, mean response and SEM, n= 9–10 trials). Responses to stimulation of each facet in isolation are shown as black solid and dashed lines

(arrowheads indicate stimulus onset). Only OFF responses are shown. **D** Distributions of summation indices as a function of ISI are shown as box plots, with ON responses in black and OFF responses in green (n = 26 facet pairs in 9 locusts). For each box, the central line indicates the median, the lower and upper boundaries are the 25^{th} and 75^{th} percentiles and the whiskers indicate the extent of the data (outliers marked by circles and triangles, respectively).

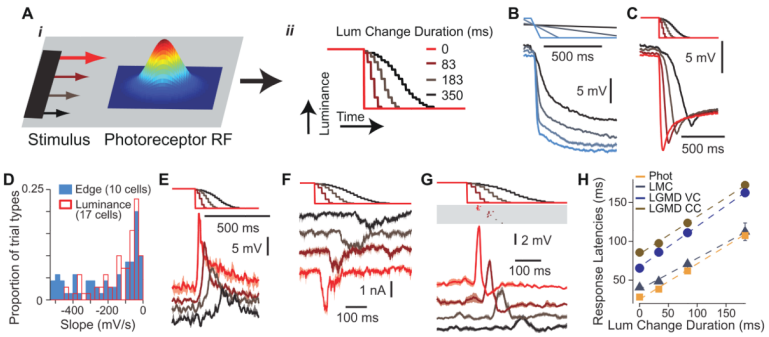

Figure 2. Single facet signaling of stimulus speed

A Model of velocity encoding by single photoreceptors. As a dark object crosses the Gaussian shaped receptive field (***i***), it produces a luminance change whose duration depends on stimulus speed (***ii***). Luminance change durations are those employed in C, E, F and G. Luminance steps occur at the refresh rate of the display. **B** Photoreceptor response to a translating dark edge moving at various speeds (20, 80, 319, and 1275 °/s). Top lines show edge position over time (maximal displacement 102°). Lines at bottom are mean responses with SEM envelopes (n = 8 trials). **C** Photoreceptor responses to single facet microscopic luminance modulation. The top stimulus traces show the luminance change over time, and the correspondingly colored traces below show the resulting photoreceptor responses. **D** Distribution of photoreceptor response slopes (calculated from 20 to 80% of the peak response) evoked by edge motion (blue; 20–1275 °/s, contrast: 0.96; 10 cells) and single facet luminance changes (red, outlined; transition duration: 1–517 ms; 17 cells). **E** Large monopolar cell (LMC) responses to similar luminance changes as in panel C (n=2–4 trials). **F** LGMD responses (I_m) to single facet luminance changes under voltage clamp (VC) at resting potential (−64 mV, n=5 trials). **G** LGMD responses to single facet luminance changes under current clamp (CC). The membrane potential (V_m) traces at the bottom have been median filtered to remove spikes prior to averaging (n = 6–7 trials). The rasters above report the timing of those spikes. **H** Peak LGMD and LMC response times, and photoreceptor response onset time (20% of peak) as a function of luminance change duration. Dashed lines show least squares linear fits, with slopes of 0.46, 0.40, 0.52, 0.49 and intercepts of 25, 37, 66 and 84 ms for photoreceptors, LMCs and the LGMD (I_m and V_m) respectively. The 95% confidence intervals on the fitted slopes were ±0.01, ±0.08, ±0.06, and ±0.08. Error bars denote SEM (photoreceptors, n = 91–100 trials; LMCs, n = 39–42; LGMD VC, n = 115–121; LGMD CC, n = 133–137).

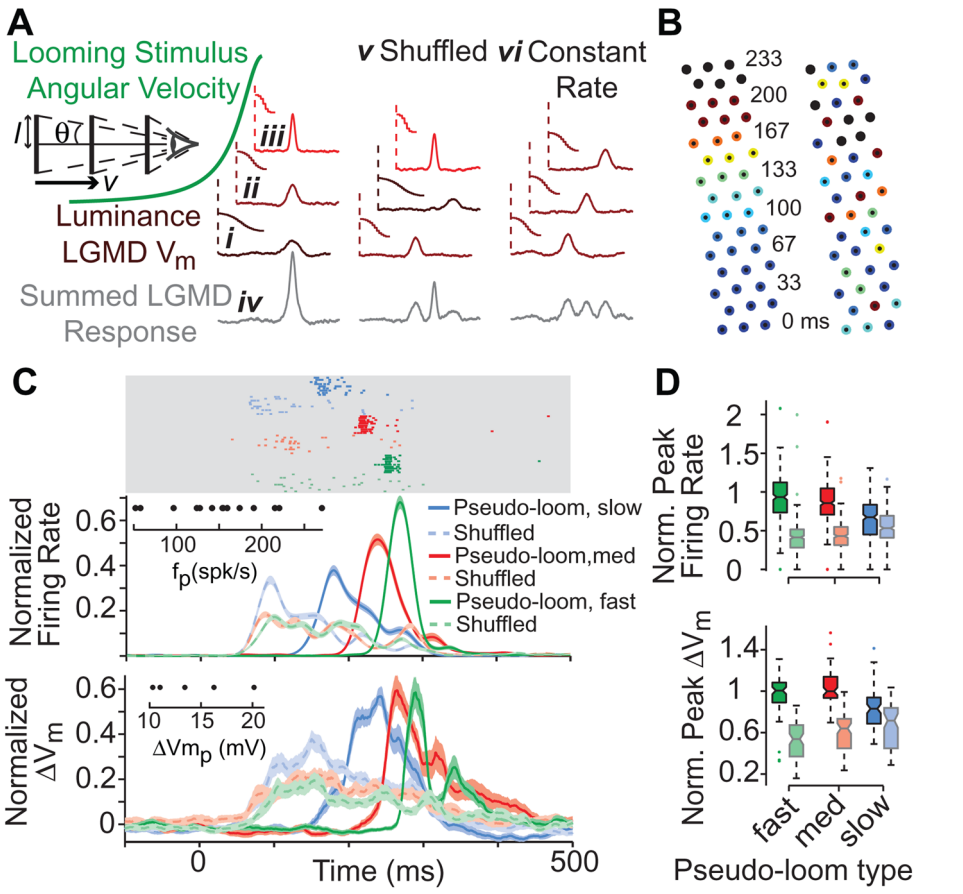

Figure 3. Temporal synchronization of LGMD excitation by accelerating sequences of luminance changes

A Temporal synchronization hypothesis and tests. The accelerating angular velocity of a looming stimulus (green) stimulates successive facets with increasingly rapid changes in luminance, leading to decreasing response latencies (***i-iii***; luminance/response pairs connected by vertical dashed lines). This sequence synchronizes excitatory inputs, resulting in strong LGMD responses (***iv***). Shuffled (***v***) and Constant Rate (***vi***) columns show stimulus manipulations used to disrupt this synchronization, by either shuffling the order of presentation, or by keeping the rates of single facet luminance changes constant. *l*: stimulus half-size, *v*: approach velocity, θ: half-angle subtended at the eye. **B** Stimulus positions used to independently target 45 facets in a pseudo-looming experiment. The numbers denote the luminance change onset times (in ms) for alternate rows of facets, while the color indicates its duration from long (cold colors) to short (hot colors; black is an instantaneous change). Left array shows pseudo-looming, with a coherent activation sequence from bottom to top (slow pseudo-loom condition); right array is corresponding shuffled condition. **C** LGMD responses to three pseudo-looms (slow, medium and fast) and the corresponding shuffled stimuli. The top rasters (light gray area) show spiking responses in one representative experiment. The traces below show normalized instantaneous firing rates (spike trains convolved with a Gaussian filter, σ=20 ms), for the recorded sample of LGMD neurons (16 animals, n=187–202 trials/condition). For each animal, single trial responses were normalized to the maximum, trial-averaged peak firing rate. The bottom traces show the normalized (as above), median filtered membrane potential in the subset of neurons for which we obtained intracellular recordings (5 animals, n=45–49 trials/condition). All traces and envelopes indicate mean and SEM. Insets show the distribution of peak firing rate (f_p)

and membrane potential change (ΔVm_p) values used for normalization. **D** Box plots showing the distributions of normalized peak firing rates and normalized peak membrane potential changes. Pseudo-looming/shuffled pairs of all types have significantly different median peak firing rates ($p_{RS}<10^{-4}$) and peak membrane potential changes ($p_{RS}<0.003$), as indicated by non-overlapping notches in box plots.

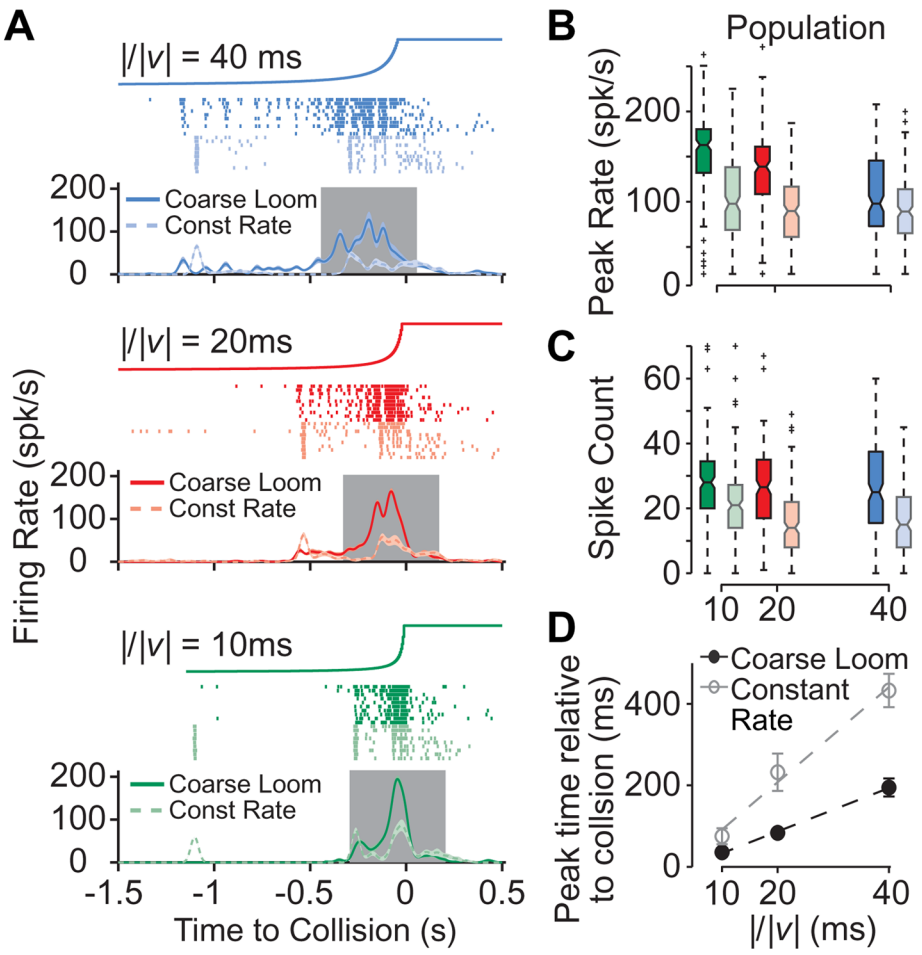

Figure 4. LGMD responses to modified looming stimuli

A LGMD responses to "coarse" and "constant rate" looming stimuli in a representative single experiment. Top traces show the stimulus angular size over time of the corresponding looming stimulus (final full angle: 85º). Rasters show LGMD spikes in each trial for coarse (saturated color) and constant rate looming (lighter color) stimuli. Correspondingly colored traces below show mean firing rates. Gray area indicates the 500 ms window centered on the LGMD peak firing rate in which spike counts were tabulated. **B, C** Box plots, formatted and colored as in Figure 3, showing the distributions of peak firing rates and spike counts for all trials pooled across the population of experiments (12 animals, n=118–122 trials/condition). Looming stimulus type had a significant effect on the peak firing rate, and the firing rates for constant rate looming were significantly lower than those for coarse looming, for all $l/|v|$ values ($p_{KW} = 10^{-20}$-10^{-5}, $p_{HSD}<0.05$). **D** Timing of the peak firing rate as a function of $l/|v|$ for coarse looming (black) and constant rate looming (gray) stimuli. Plotted circles are population mean times, with error bars indicating SEM. Dashed lines show linear fits to the data, with slopes of 5.3 and 11.7 and intercepts of −20 and −19 ms for looming and constant rate stimuli, respectively.